
Article:
Dagrada, Gianpaolo, Rupel, Katia, Zacchigna, Serena et al. (8 more authors) (2018) Self-Assembled Nanomicelles as Curcumin Drug Delivery Vehicles: Impact on Solitary Fibrous Tumor Cell Protein Expression and Viability. MOLECULAR PHARMACEUTICS. pp. 4689-4701. ISSN: 1543-8384

https://doi.org/10.1021/acs.molpharmaceut.8b00655

---

molecular pharmaceutics

Article

Self-Assembled Nanomicelles as Curcumin Drug Delivery Vehicles – Impact on Solitary Fibrous Tumor Cell Protein Expression and Viability

Gianpaolo Dagrada, Katia Rupel, Serena Zacchigna, Elena Tamborini, Silvana Pilotti, Adalberto Cavalleri, Loryn E. Fechner, Erik Laurini, David K. Smith, Silvia Brich, and Sabrina Pricl

Mol. Pharmaceutics, **Just Accepted Manuscript** • DOI: 10.1021/acs.molpharmaceut.8b00655 • Publication Date (Web): 04 Sep 2018

ACS Publications

is published by the American Chemical Society. 1155 Sixteenth Street N.W., Washington, DC 20036

Self-Assembled Nanomicelles as Curcumin Drug Delivery Vehicles – Impact on Solitary Fibrous Tumor Cell Protein Expression and Viability

Gianpaolo Dagrada[a], Katia Rupel[b,c], Serena Zacchigna[c], Elena Tamborini[a], Silvana Pilotti[a], Adalberto Cavalleri[d], Loryn E. Fechner[e], Erik Laurini[f], David K. Smith[e], Silvia Brich[a,*,#] and Sabrina Pricl[f,#]

[a]Laboratory of Molecular Pathology, Department of Pathology, Fondazione IRCCS Istituto Nazionale dei Tumori, 20133 Milan, Italy

[b]Division of Oral Medicine and Pathology, Dental and Maxillofacial Surgery Clinic, Ospedale Maggiore, Piazza dell'Ospitale 1, 34129 Trieste, Italy

[c]Department of Medical, Surgical and Health Sciences, University of Trieste, Strada di Fiume 447, 34149 Trieste, Italy

[d]Endocrinology Laboratory, Epidemiology and Prevention Unit, Fondazione IRCCS Istituto Nazionale dei Tumori, 20133 Milan, Italy

[e]Department of Chemistry, University of York, Heslington, York, YO10 5DD, United Kingdom

[f]Molecular Biology and Nanotechnology Laboratory (MolBNL@Units), DEA, University of Trieste, 34127 Trieste, Italy

[#]co-last authors

*Corresponding author: Silvia Brich, phone: +39 0223903016, e-mail: silvia.brich@istitutotumori.mi.it

Abstract

Solitary Fibrous Tumors (SFTs), rare soft tissue sarcomas that rely on several Epithelial-Mesenchymal-Transition (EMT) protein regulators for invasion/metastatic progression. Curcumin (CUR) has several pharmacological activities, including anticancer activity and ability to suppress the EMT process. However, poor absorption, rapid metabolism and side effects at high doses limit the clinical applications of CUR. Here we present the results obtained by treating SFT cells with free CUR and three different CUR-loaded nanomicelles (NMs), each of which has its surface decorated with different ligands. All CUR-loaded NMs were more efficient in suppressing SFT cell viability and expression of EMT markers than CUR alone. Combined treatments with the pan-histone deacetylase dual inhibitor SAHA revealed a differential ability in inhibiting EMT markers expression and SFT cell invasiveness, depending on the NM-ligand type. Finally, combinations of photodynamic therapy and CUR-loaded NM administrations resulted in almost complete SFT cell viability abrogation 24 hours after laser irradiation.

Keywords

Curcumin; Self-assembled nanomicelles; Solitary Fibrous Tumor; Anticancer Activity; Photodynamic Therapy

Background

Solitary fibrous tumor (SFT) is a mesenchymal tumor of fibroblastic type[1,2] in which the gene fusion NAB2-STAT6 has been identified as the molecular hallmark.[3] Most SFTs present as well-defined, slow-growing masses that can be cured by surgery. 10-20% of SFTs behave more aggressively, with local recurrence and/or distant metastasis for which systemic therapy is the clinical option.[1,4-6] Advanced SFTs are more sensitive to the tyrosine kinase inhibitor (TKI) Sunitinib rather than to other TKIs (e.g., Sorafenib or Pazopanib)[7-9] or to monoclonal antibodies (Bevacizumab).[10] However, Sunitinib anti-tumor effect is transient, autophagy promoted by prolonged treatment likely acting as the mechanism leading to drug resistance.[11] Also, SFTs are characterized by subpopulation of cells with stem-like properties notoriously refractory to chemotherapeutics.[12] Literature suggests this cell pool may originate from fully differentiated cells via Epithelial-Mesenchymal-Transition (EMT), in which a series of protein hallmarks including SLUG, TWIST, EZH2, YY1 and integrinβ3 play a crucial role in invasion/metastatic progression.[13] The medicinal benefits of curcumin (CUR, Figure 1 left), a natural polyphenolic compound derived from *Curcuma longa*, are well known.[14] Anti-inflammatory and antioxidant properties of CUR, along with immunomodulatory, proapoptotic, and antiangiogenic effects, are the main mechanisms underlying CUR anti-tumor activity. Moreover, CUR has a remarkable ability to negatively interfere with the EMT process in many cancer types.[15] Regrettably, CUR low water solubility and poor pharmacokinetics are essential factors that severely curtail its effective application in cancer therapy.[16,17] An obvious approach to circumvent these issues is the use of nanocarriers for CUR encapsulation, transport and delivery.[17,18] In the synthetic nanovector arena, we reported a variety of self-assembled multivalent (SAMul) nanostructures which achieved high affinity binding to biological polyanions (e.g., DNA and heparin).[19-26] We reasoned that the hydrophobic interiors of these SAMul nanomicelles (NMs) should be able to encapsulate CUR and deliver it to SFT cells, and this led to the design of this current study. In particular, we used a small family of SAMul entities (Figure 1 center) in which the ligand groups displayed on the surface of the relevant NMs

were subtly varied,[23] in order to determine whether molecular-scale programming of the nanovector could have an impact on cellular uptake, release and subsequent anti-cancer activity of CUR.

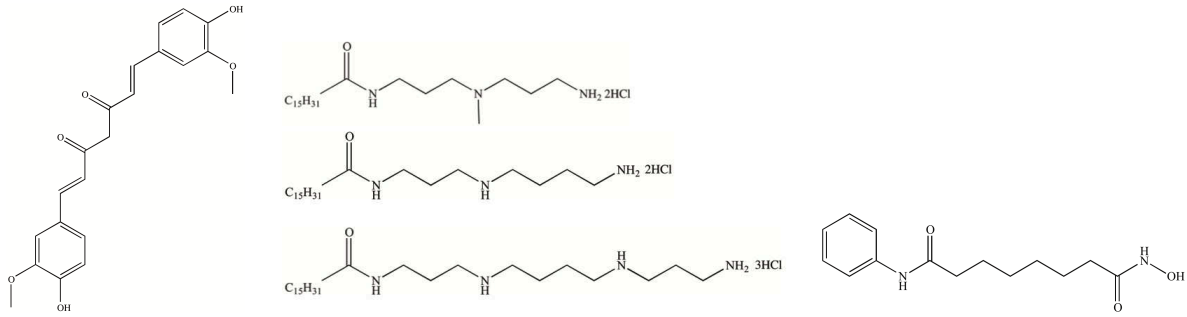

Figure 1. Chemical structure of curcumin (left), the three SAMul chemical entities DAPMA, SPD, and SPM (center), and of the pan-hystone deacetylase inhibitor suberoylanilide hydroxamic acid (SAHA, right).

Accordingly, three different types of CUR-loaded SAMul NMs were prepared, characterized, and the relevant *in vitro* CUR release was measured. The effects of these three CUR-nanoformulations on SFT cells viability and invasiveness were assessed, and the expression of EMT markers was determined.

Given the evidence that the NAB2/STAT6 fusion protein interacts with histone deacetylase2 (HDAC2) activity in SFTs, the outcomes of an *in vitro* combined treatment with CUR-loaded NMs and the pan-HDAC inhibitor SAHA (Vorinostat)[27] (Figure 1 right) were next investigated. Finally, as photodynamic therapy (PDT) is increasingly being recognized as an attractive, alternative treatment modality for superficial cancers,[28] we surmised that combining PDT with CUR-NMs delivery could further potentiate CUR anticancer activity in SFT cells. Thus, CUR-NMs/PDT combined treatments were also carried out. All experiments described above were performed in parallel using free CUR, and the relative performance of free- and nano-delivered CUR is presented and discussed.

Experimental Section

Reagents

Culture media Dulbecco's Modified Eagles Medium (DMEM) and its supplements containing antibiotics and fetal bovine serum (FBS) were purchased from Gibco Invitrogen Corporation

(USA). Curcumin and SAHA were purchased from Sigma Aldrich (Italy).

Stabilized SFT cell line

The primary SFT cell line was stabilized by retroviral delivery of SV40 large T-antigen (pwzl-neo large T-Ag) performed in accordance with standard procedures.[11] The nuclear expression of STAT6 in formalin fixed paraffin embedded (FFPE) cells was verified by immunohistochemistry (IHC).

Synthesis of DAPMA, SPD, and SPM-based self-assembling amphiphilic molecules

C_{16}-N,N-di-(3-aminopropyl)-N-methylamine (DAPMA), C_{16}-spermidine (SPD), and C_{16}-spermine (SPM) SAMul molecules were available from our previous work. Their synthesis, purification and characterization are reported in detail in our previous work.[23]

Preparation of CUR-loaded nanomicelles

DAPMA, SPD, and SPM nanomicelles (NMs) used to encapsulate CUR were obtained by the film dispersion method.[19] Accordingly, 0.32 mg of CUR were dissolved in 1 mL of mixed solvent (chloroform:methanol = 3:2) (vol/vol). The drug was then mixed with 3 mg of DAPMA, SPD, or SPM, respectively, in 3 mL of mixed solvent. The solvent was removed by vacuum rotary evaporation to form a dry film. The dried film was then hydrated with HEPES buffer (10 mM, pH 7.4) at 60°C for 30 minutes under stirring. Free CUR was separated by filtration through 0.45 μm polycarbonate membrane (Millipore Co., USA). Incubation overnight at 4°C was followed by 9 hours of dialysis (changing distilled water every hour) using a membrane with molecular weight cut-off of 2000 Da. The product in the dialysis tube was then lyophilized (SpeedVac, Thermo Fisher, USA). CUR encapsulation efficiency in each micelle type (%, = (weight of loaded CUR /total CUR weight) x 100)[19] was quantified by UV-vis spectroscopy (Ultrospect 3100PRO, Amersham Biosciences, UK) at 420 nm.

Characterization of NMs Using Dynamic Light-Scattering (DLS)

The size distribution and zeta potential of empty and CUR-loaded NMs were determined by DLS measurements using a Zetasizer Nano-ZS (Malvern, UK). All reported experimental results were performed in triplicate and reported as mean value ± standard deviation (SD).

In vitro CUR release

The release of CUR from DAPMA, SPD and SPM loaded NMs was performed using the dialysis method. Accordingly, a known quantity (1.0 mg/mL) of each CUR-loaded NM was dispersed in 10 mM PBS at pH 7.4 and then transferred into the dialysis membrane tubes (molecular weight cut-off 3000 Da). Since CUR is only sparingly soluble in aqueous media, the release study was carried out by immersing the tube in a beaker containing 50 mL of 50:50 (v/v) methanol: water solution to facilitate sink-like conditions and stirred constantly at 37 °C for 0, 1, 2, 4, 6, 8, 10, 12, and 24 h. At each time point, 1 mL of solution was withdrawn from the release medium and replaced with fresh PBS. CUR content was again determined using the UV-vis DS11-FX spectrophotometer (DeNovix Inc., USA) at 420 nm.

Cell treatments with CUR and CUR-loaded NMs

The SFT cell line was grown in DMEM containing 5%FBS. Cells were maintained as monolayer in a humidified atmosphere (5% CO_2, 37°C). After 72h, culture medium was replaced with treatment medium containing different concentrations of free or CUR-loaded NMs.

Combined CUR/SAHA and CUR-loaded NMs/SAHA treatments

Suberoylanilide hydroxamic acid (SAHA) was added to CUR or CUR-loaded NM treatments of SFT cells. Optimal SAHA concentration for combination experiments was determined by dispensing SFT cells with 5 μM of SAHA for 24 and 48h (5% CO_2, 37°C).

SFT cell CUR uptake and phalloidin immunofluorescence (IF) in combined treatments

SFT cells ($3x10^5$) were seeded in each plate using DMEM supplemented with Penicillin/Streptomycin/Gentamicin/10%FBS and incubated (37°C, 5% CO_2) for 3 days before any treatment, without medium restoring. Autoclaved coverslips were added to each plate in order to allow cells to grow on them. SFT cells were treated as described above with CUR, CUR-loaded NMs, and SAHA. The last day of treatment, coverslips were removed and then fixed with methanol (CUR uptake assay) or paraformaldehyde (phalloidin staining). The distribution of CUR inside SFT cells was observed by fluorescence microscopy at an excitation wavelength of 488 nm. Phalloidin

(1:200 in DPBS, 2 hours incubation, Alexa Fluor) was used to observe actin fiber changes after SAHA treatments. DAPI (blue signal) was used to counterstain nuclei. Representative fields were captured with a DM6000FS fixed stage fluorescence microscope (Leica, Germany).

Cell viability assays

Cell viability was determined by the 3-(4,5 dimethylthiazol-2-yl)-2,5-diphenyl-tetrazolium bromide (MTT, Sigma Aldrich, Italy) assay. Cultures were initiated in 96-wells plates at a density of 5×10^3 cells per well. After 72 h incubation, cells were treated with different concentrations of free CUR, CUR-loaded NMs, or combined treatment dosed and cultured for 24 h. Next, 20 μL of MTT reagent was added to each well and incubated for 4h at 37°C, 5% CO_2 in the dark. The supernatant was aspirated and then 100 μL of DMSO were added under gentle stirring. The absorbance per well was measured at 550 nm (Infinite M1000, TECAN, Switzerland), and normalized to the absorbance of wells containing untreated cells. The cytotoxicity of blank DAPMA, SPD, and SPM NMs in two non-cancer cell lines (normal human primary lung fibroblasts, HLF, ATCC® PCS-201-013, and normal human primary prostate epithelial cells, HPrEC, ATCC® PCS-440-010, ATCC, Manassas VA, USA) was also evaluated by the MTT assay. To this purpose, cells were seeded and incubated with 75 μM, and 100 μM of each blank NM under the same experimental conditions. All cytotoxicity results were obtained from three independent measurements and are expressed as mean value ± standard deviation (SD).

Invasion assay

Transwell membrane (Corning, Japan) coated with matrigel (BD Biosciences, USA) was used for the invasion assay.[29] After collecting and centrifuging, SFT cells were re-suspended at $1.25\text{x}10^5$ cells/mL. Then, 2 mL of cell suspension ($2.5\text{x}10^5$ cells) were seeded to upper wells of pre-coated Transwell chambers. Cells were then incubated with 10 μM, 20 μM and 50 μM CUR re-suspended in DMEM. DMEM alone was used as control. In parallel, 500 μL of DMEM+10%FBS was placed in the lower chambers as a chemo-attractant. After 24 h incubation, cells in the upper chamber were removed, fixed in methanol and stained with crystal violet. Finally, cells attached through the

matrigel were counted in five random (center and borders) microscope fields (200x), and averaged.

Biochemical analyses

Proteins were extracted as previously described.[30] Protein (20 μg of total protein lysate per sample) was subjected to western blot (WB) analysis using standard protocols. EZH2 (#5246) and SLUG (#9585) antibodies were purchased from Cell Signaling Technology (USA); YY1 (ab109237), integrinβ3 (ab75872) and c-myc (ab32072) antibodies were obtained from Abcam (USA). Actin (A2228), used to normalize protein expression, was purchased from Sigma Aldrich (Italy). The secondary antibodies anti-rabbit and anti-mouse were purchased from Santa Cruz Biotechnology (USA).

CUR and CUR-NMs/photodynamic therapy (PDT) combined treatments

SFT cells incubated with free CUR and CUR-loaded NMs at the same concentrations employed in the toxicity assays reported above were exposed to a 445 nm blue laser light (power density 150 mW/cm^2, estimated average fluency of 9 J/cm^2) (Klaser, Eltech K-Laser, Italy). The distance between the laser and the 96-wells plates was optimized to enable an identical distribution of light on each well. Further non-irradiated 96-well plates were used as control). After laser treatments, cells were kept at 37°C, 5% CO_2 for 1 h. Then, 10 μM 2',7'-dichlorofluorescin diacetate (Thermo Fischer Scientific, USA) were added to each well, followed by 30 minutes incubation at 37°C, 5% CO_2 to evaluate Reactive Oxygen Species (ROS) production. The dye solution was then replaced with Dulbecco's Phosphate Buffered Saline (DPBS, Sigma Aldrich, Italy) and plates were read by means of a fluorescence spectrophotometer (EnVision, 2104 Multilabel Reader, PerkinElmer, USA) at 520 nm. Moreover, MTT analyses were carried out on the same plates after DPBS washing.

Results

Free CUR treatments reduce SFT cell viability and EMT-markers expression

Free CUR uptake by SFT cells was confirmed by fluorescence microscopy (Figure 2A, left). The intensity of the green fluorescent signal proportionally increased with increasing concentrations of

CUR (Figure 2A, right). A concentration-dependent cell viability behavior was observed (Figure 2B): 10 μM treatment induced no variation in cell viability, 20 μM resulted in a minimal decrease in cell viability, while 50 μM drastically reduced the number of viable cells to less than 20%. Also, 10 μM free-CUR exposure resulted in a 50% reduction in cell invasion, while a 99% reduction was achieved with 50 μM CUR (Figure 2C). Concomitantly, the expression of the EMT markers was significantly reduced after CUR treatment (50 μM, 24 h) (Figure 2D). Of note, c-Myc and SLUG expression was already reduced after 24 h treatment with 20 μM CUR, and the low expression of these two proteins was maintained in the second day of treatment (Figure 2D).

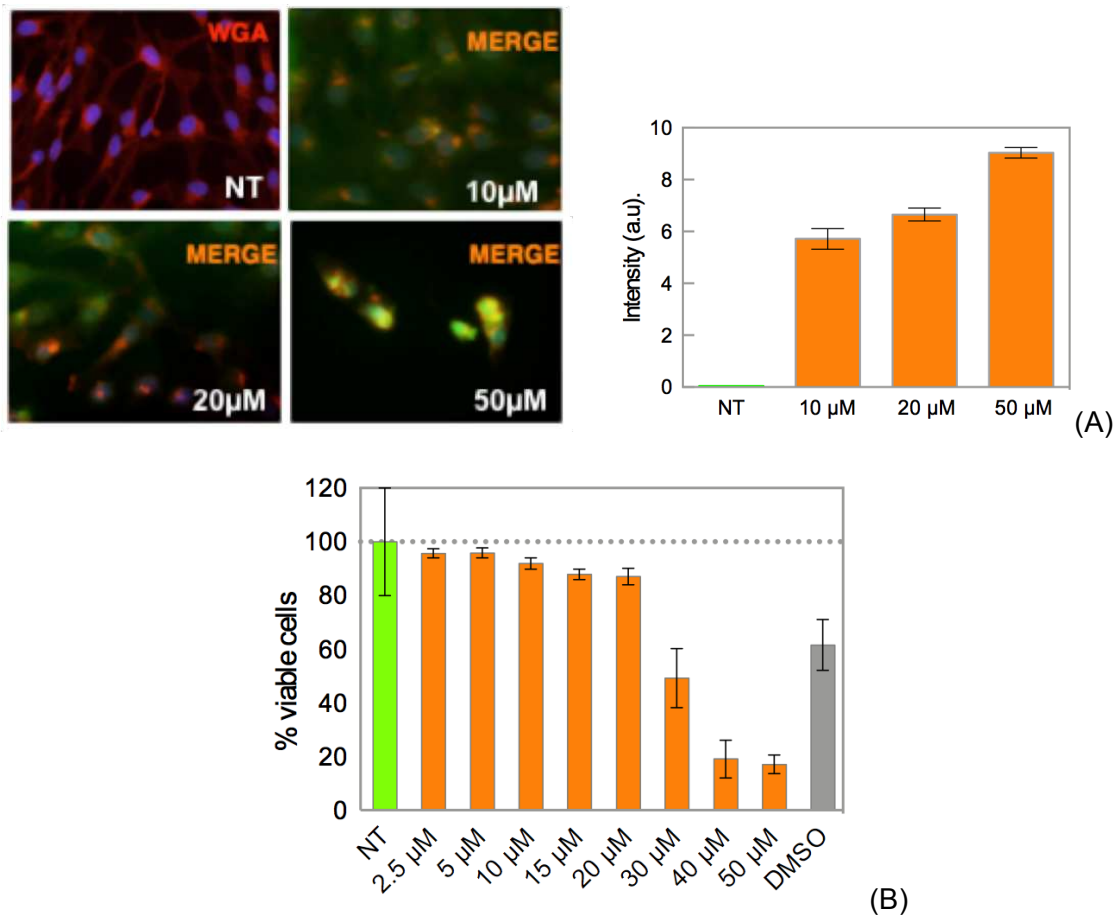

Figure 2. SFT cells treated with CUR. (A) Left: representative confocal images of free CUR uptake (24 hr) in SFT cells stained with red (WGA Alexa Fluor 546) for plasma membranes and blue (DAPI) for nuclear counter-stain. CUR auto-fluorescence captured at 488 nm (green) wavelength (magnification 40x). Right: quantitative analysis of the green signal intensity for the images in the right panel. NT _= non-treated cells. Data represent the average of three independent experiments ± the standard deviation. (B) Viability of SFT cells (24 h) treated with CUR. NT: non-treated cells. (C) Representative fields of invasive SFT cells on membrane (magnification 200X, left panel) and average number of migratory cells per field (right panel) after CUR treatment. Data represent the average of three independent experiments ± the standard deviation. (D) WBs for EMT marker expression (actin as control) after CUR treatment. Actin is used as control.

Preparation and physico-chemical characterization of CUR-loaded NMs

The compounds DAPMA, SPD, and SPM used in this work bore a different, positively charged ligand moiety coupled to a C_{16}-alkyl chain[23] (Figure 1B). Using the film dispersion method, all three molecules formed similar-sized nanoassemblies, both in the absence and presence of CUR, as detected by DLS (Figures 1SA-F). The NM average dimensions and their zeta-potentials were only slightly affected by CUR encapsulation (Table 1S). The drug-encapsulation efficiency (EE, %) and the drug loading capacity (DL, %) of all three NMs were also comparable (EE = 10-13% and DL = 11-16% Table 1S). All three NMs consistently showed lower CUR release when compared to free CUR (Figure 2S): while approximately 91% of CUR was released in the first 6 hours of dialysis, only 43 to 50 % of the loaded CUR was released from the three loaded NMs in the same time interval. The cumulative release of CUR from the DAPMA, SPD, and SPM NMs was 78.31 ± 3.18%, 77.23 ± 4.11%, and 66.83 ± 5.02%, respectively.

Nanomicelles loaded with CUR are more effecting in reducing cell viability and invasiveness

The amount of CUR detected inside SFT cells after NM delivery was comparable to that observed upon treatment with free CUR at 50 μM. Notably, however, the nominal CUR concentrations actually being administered in the case of NMs were considerably reduced (Figure 3A). At any given drug concentration, all three CUR-loaded NMs were remarkably more effective in their cytotoxic activity than the corresponding free-CUR system (Figure 3B). Additionally, the viabilities of SFT and two non-cancer cell lines cultured in the presence of all three blank NMs were in the range 79-93% at the highest concentration tested (100 μM, Figure 3C); accordingly, the three NMs are endowed with little intrinsic cytotoxic activity in their own right.

CUR-loaded NMs also inhibited cell invasiveness; yet, in this case cell invasiveness inhibition was

induced at much lower CUR concentrations (Figure 3 D-F). The inhibition of SFT cell migration by CUR-SPM (500 nM) was somewhat less effective than that achieved with CUR-DAPMA and CUR-SPD delivering the same CUR concentration, in line with the slower CUR release (Figure 2S) and the lower SFT cytotoxic effect associated with the CUR-SPM nanomicelles (Figure 3).

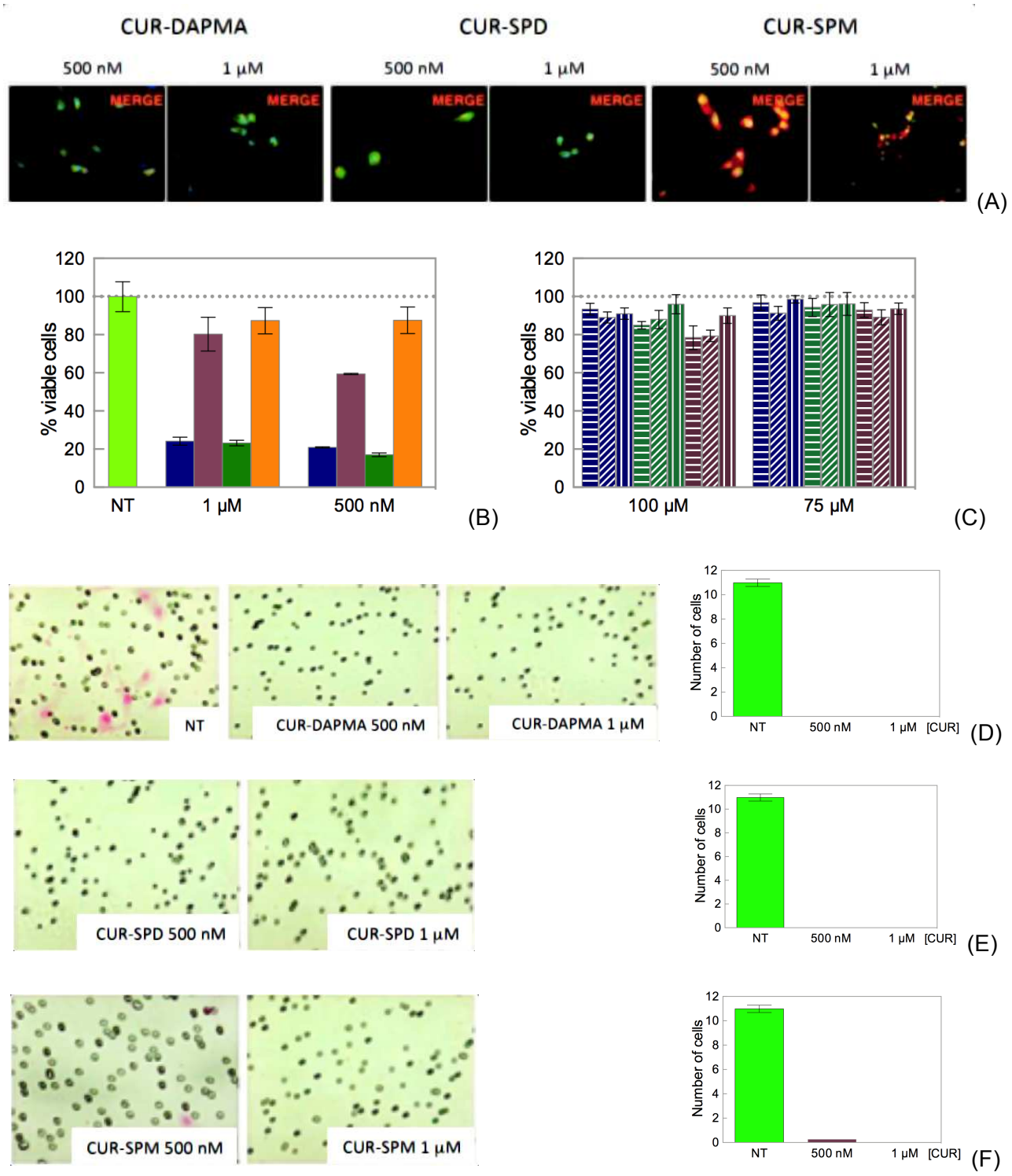

Figure 3. SFT cells treated with CUR-loaded NMs. (A) Confocal images of NM-delivered CUR uptake in SFT cells (conditions as in Fig. 2A). (B) Viability of SFT cells (24 h) treated with CUR-DAPMA (dark blue), CUR-SPD (dark green), CUR-SPM (dark plum) NMs and free CUR. NT = non-treated cells (green bar). (C) Cytotoxicity of blank

DAPMA (patterned dark blue), SPD (patterned dark green) and SPM (patterned dark plum) NMs in SFT (vertically striped bars) and two non-cancer cell lines: normal human primary lung fibroblasts (HLF, horizontally striped bars) and normal human primary prostate epithelial cells (HPrEC, diagonally striped bars). Representative fields of invasive cells on membrane (magnification 200X, left panels) and average number of migratory cells per field (right panels) after CUR-DAPMA (D), CUR-SPD (E), and CUR-SPM (F) NM treatments. NT = non-treated cells. Data represent the average of three independent experiments ± the standard deviation.

Inhibition of EMT markers expression

WB analyses (Figure 4) revealed that SFT cells treated with CUR-loaded NMs expressed different amounts of EMT markers. CUR-DAPMA and CUR-SPD NMs treated cells expressed significantly lower amounts of EZH2 compared with those receiving CUR-SPM. Similarly, YY1 expression was slightly reduced after 1μM CUR-DAPMA and CUR-SPD treatments but not by CUR-SPM. This is in agreement with the results above which suggested that SPM was a less effective delivery vehicle for CUR. Notably, CUR-SPD was the only system able to strongly inhibit c-Myc expression. On the other hand, SLUG expression was abolished after treatment with all three different NMs. Finally, integrin β3 expression was exclusively affected by CUR-SPD treatment. Overall, the CUR-SPD system appears to be the most effective drug-NM combination in terms of inhibiting the expression of EMT markers.

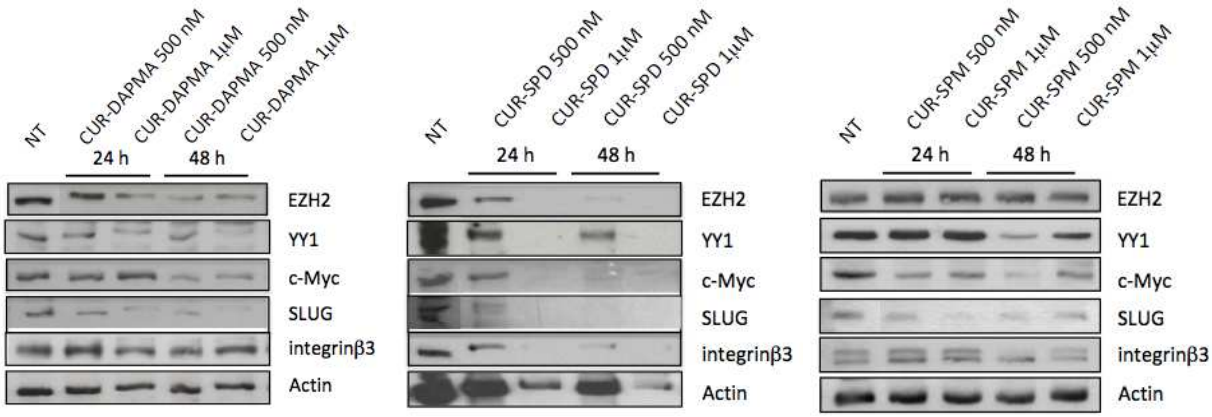

Figure 4. Western blots for EMT markers expression following treatments with CUR-DAPMA (left), CUR-SPD (center), and CUR-SPM (right) NMs. Actin is used as control.

Free CUR and SAHA combined treatments

In order to verify any synergistic effect between the cytotoxic action of CUR and the HDAC

inhibitor SAHA, combination experiments were performed. After 24h of combined treatment, no significant reduction in SFT cell viability was observed. Extending treatment to 48h revealed that, while SAHA exerted a weak dose-dependent cytotoxic effect *per se* (EC_{50} = 2.7 μM), when co-administered with CUR this effect was reversed, particularly at the highest CUR dose (Figure 5A). Phalloidin IF carried out after SAHA/CUR combined treatment underlined a partial reversal of the mesenchymal phenotype, evidenced by a shift from spindle shaped cells with visible actin stress fibers to predominantly cuboidal shape cells after 24 h of treatment (Figure 5B-D). CUR combined with SAHA showed no increase in therapeutic efficacy when compared with the corresponding CUR treatment alone (Figure 5E). To determine whether SAHA could enhance the effect of CUR on HDAC2 and MMP2 expression, 5 μM SAHA was administered in combination with different CUR concentrations for 24-48 h. The combined treatment increased both HDAC2 and MMP2 levels. On the other hand, SAHA alone led to a decrease of MMP2 expression (Figure 5F).

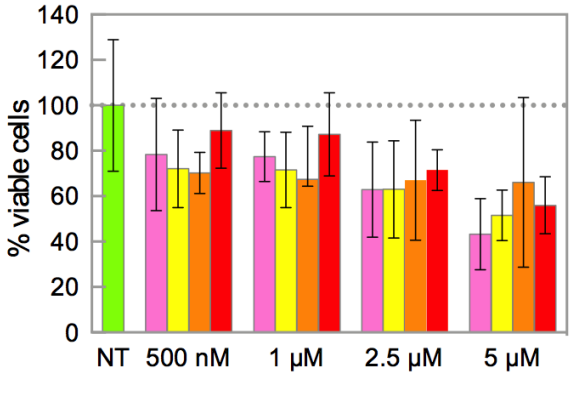

(A)

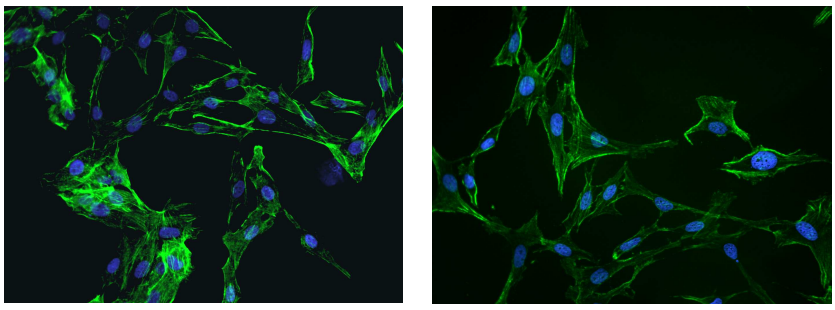

(B)

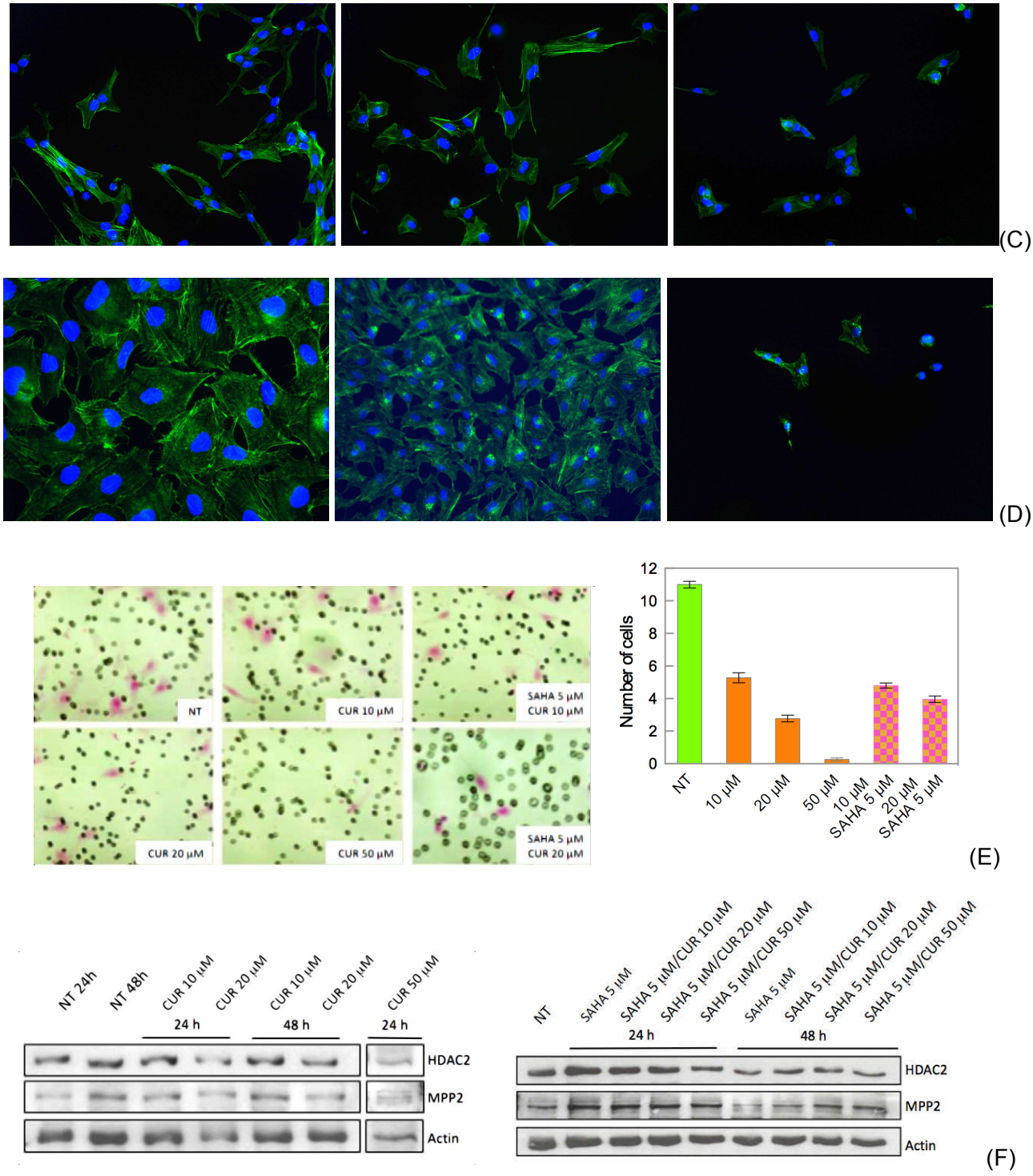

Figure 5. SFT cells treated with CUR/SAHA. (A) Viability of SFT cells (24 h) treated with different SAHA concentrations (marked on the x-axis) alone (pink bars) or combined with CUR (10 μM, yellow bars; 20 μM, orange bars, and 50 μM, red bars). NT = non-treated cells (green bar). Morphological change of SFT cells induced by SAHA, CUR and combined treatments (CUR /SAHA) after 24/48 h visualized by phalloidin IF (Green (Alexa Fluor 488): actin filaments; blue (DAPI): nuclear counter-staining, representative fields, magnification 100X): (B) non-treated cells (left), CUR -/SAHA 5 μM (right). (C) CUR 10 μM/SAHA - (left), CUR 20 μM/SAHA - (center), CUR 50 μM/SAHA - (right). (D) CUR 10 μM/SAHA 5 μM (left), CUR 20 μM/SAHA 5 μM (center), CUR 50 μM/SAHA 5 μM (right). (E) Suppression of SFT cells invasiveness by CUR alone and in combination with SAHA: representative fields of invasive cells on membrane (magnification 200X, left) and average number of migratory cells per field (right). CUR, orange bars; CUR/SAHA: orange-pink checked bars. NT = non-treated cells (green bar). Data represent the average of three independent experiments ± the standard deviation. (F) Western blots for HDAC2 and MMP2 expression following CUR alone (left) and combined CUR/SAHA (right) treatments. Actin was used as control.

CUR-NMs and SAHA combined treatments

To determine the sensitivity of SFT cells to the cytotoxic/cytostatic effects of the combined CUR-NM/SAHA treatment, cells were incubated with the three CUR-loaded NMs in combination with 5 μM SAHA for 24 h. Unlike free CUR/SAHA (Figure 6A), the SAHA/CUR-SPD combined administration induced cell death (Figure 6B). Moreover, on 24h treatment with SAHA/CUR-SPD, the SFT cells exhibited partial reversal of the mesenchymal phenotype, characterized by a shift from spindle shaped cells with visible actin stress fibers to predominantly epithelial-like shape cells. Phalloidin signal intensity progressively decreased after treatments while SFT cells assumed more epithelial-like features before death (Figure 6D-F). Conversely, the combined SAHA/CUR-DAPMA and SAHA/CUR-SPM treatments stimulated cell growth (Figure 6B-C).

CUR-SPD and CUR-SPM NMs, administered in combination with SAHA, also significantly inhibited cell invasiveness compared to untreated samples. Contrarily, after SAHA/CUR-DAPMA combined treatment the number of cells endowed with invasive potential remained very high (Figure 6G-I). This was an unexpected result, since treatment with CUR-DAPMA alone had abolished this invasiveness (Figure 3D).

Lastly, while all three CUR-loaded NMs did not significantly affect the expression of HDAC and MMP2 *per se* (Figure S3), the combined treatment SAHA(5 μM)/CUR-DAPMA(1 μM) reduced HDAC2 expression. In contrast, HDAC2 expression levels were not affected by SAHA/CUR-SPD or SAHA/CUR-SPM treatments at the same concentrations, while HDAC2 expression increased after treatment with SAHA (5 μM) alone or in combination with CUR-SPD (500 nM). MMP2 expression decreased after all SAHA/CUR-NM combined treatments. In particular, a significant decrease in MMP2 expression was observed after administration of SAHA/CUR-SPD and SAHA/CUR-SPM (Figure 6J-L).

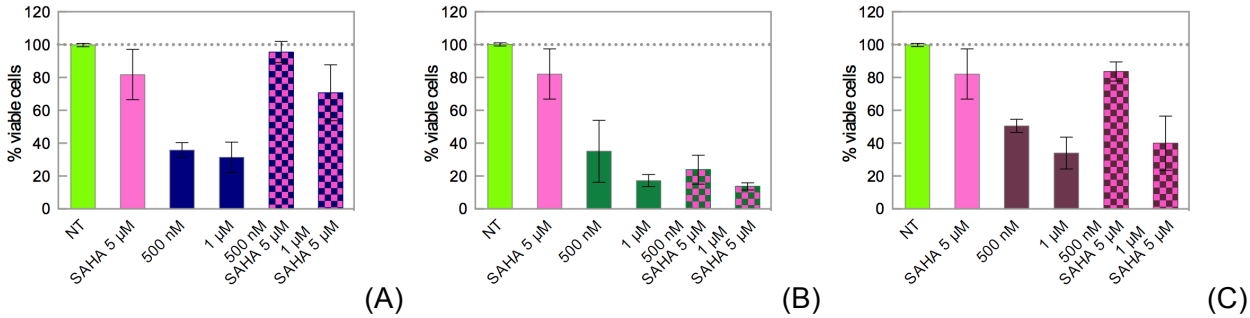
% viable cells
120
100
80
60
40
20
0
NT
SAHA 5 μM
500 nM
1 μM
500 nM SAHA 5 μM
1 μM SAHA 5 μM

(A) (B) (C)

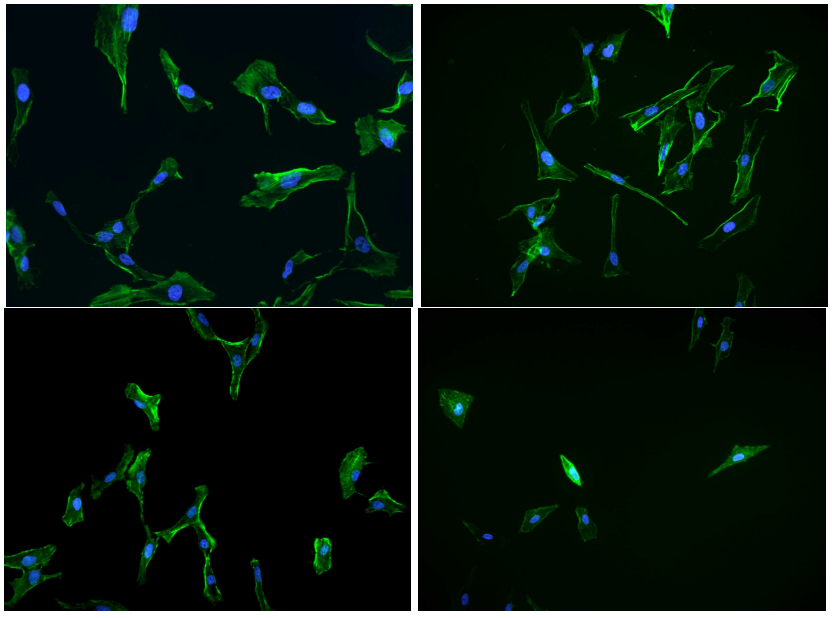

(D)

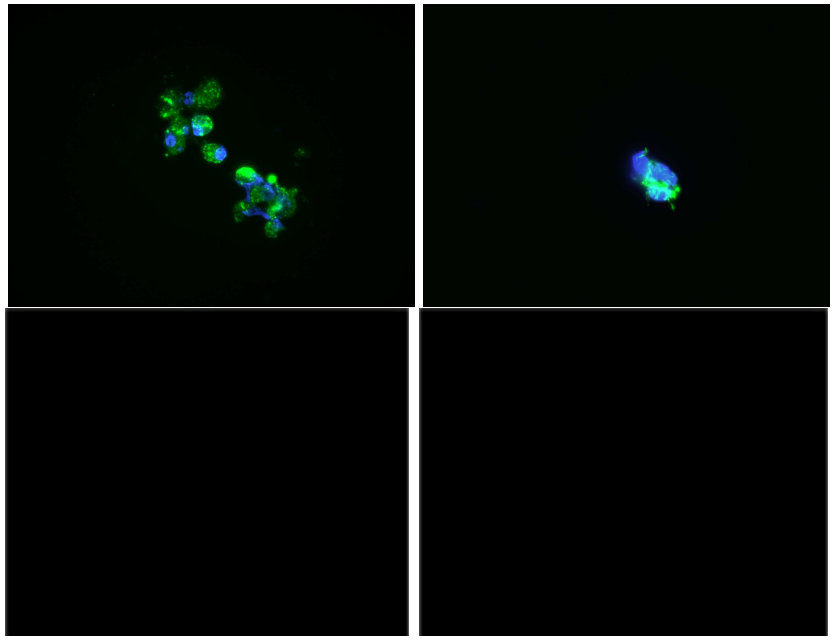

(E)

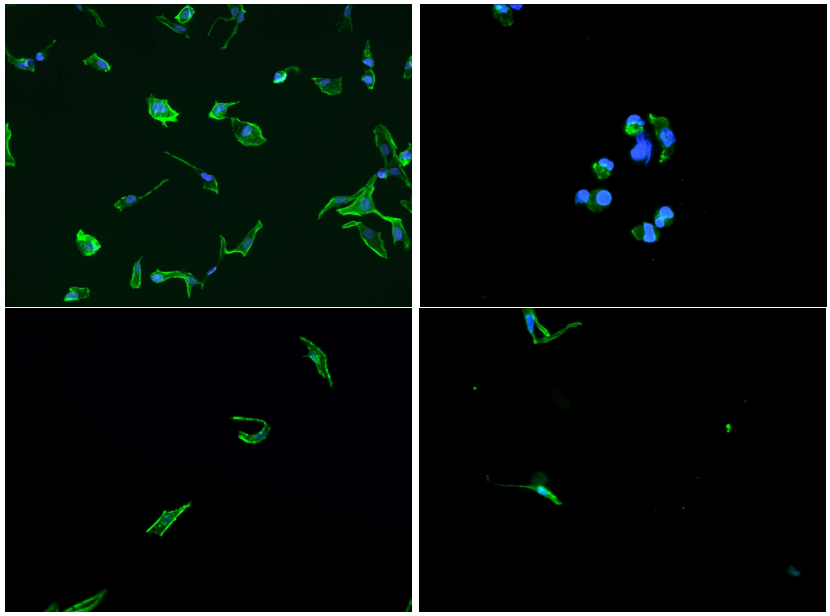

(F)

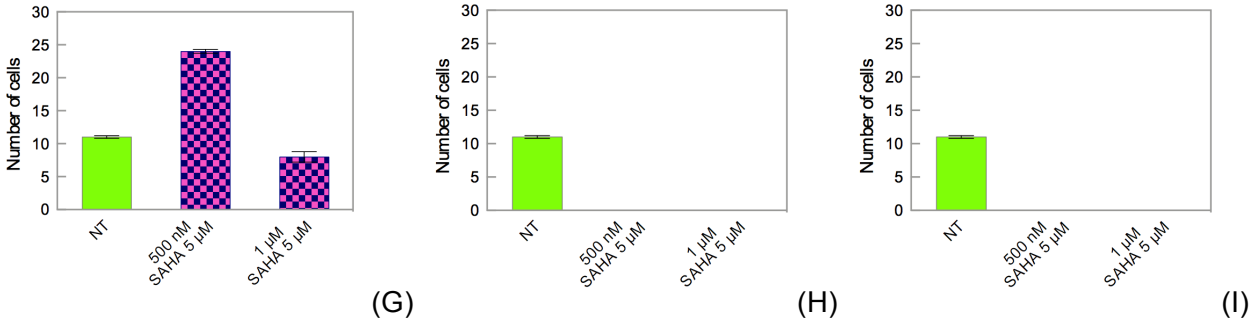

(G) (H) (I)

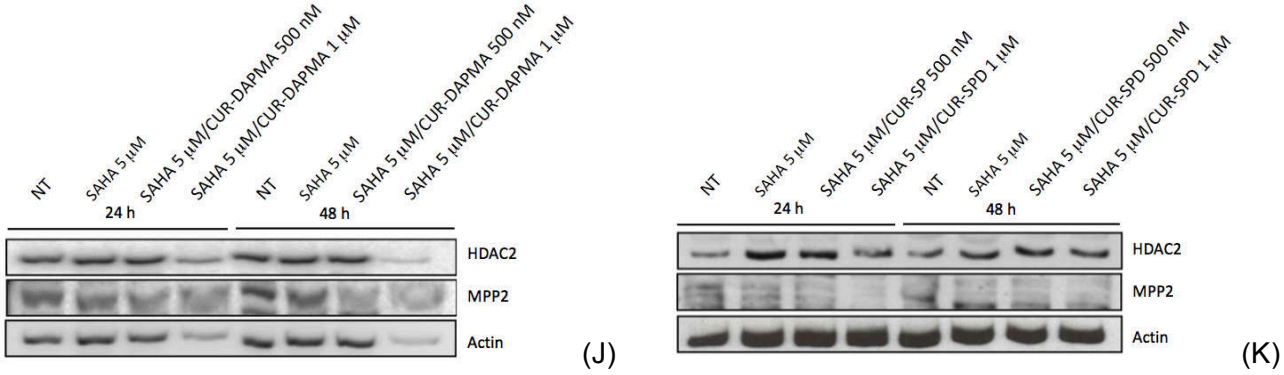

(J)

(K)

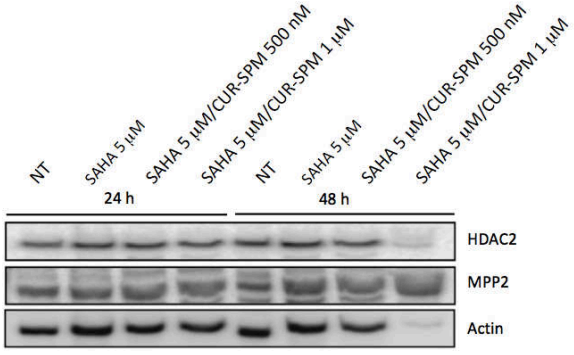

(L)

Figure 6. SFT cells treated with CUR-loaded NMs/SAHA. Viability of SFT cells (24 hr) treated with SAHA alone (pink bars), (A) CUR-DAPMA alone (dark blue bars) and in combination with SAHA (dark blue/pink checked bars); (B) CUR-SPD alone (dark green bars) and in combination with SAHA (dark green/pink checked bars); (C) CUR-SPM alone (dark plum bars), and in combination with SAHA (dark plum/pink checked bars). NT = non-treated cells (green

bars). Morphological change of SFT cells induced by combined SAHA/CUR-DAPMA (D), SAHA/CUR-SPD (E), and SAHA/CUR-SPM (F) treatments after 24h and 48h visualized by phalloidin IF (Green (Alexa Fluor 488): actin filaments; blue (DAPI): nuclear counter-staining, representative fields, magnification 100X). Suppression of SFT cells invasiveness by combined SAHA/CUR-loaded NMs treatments: average number of migratory cells per field after SAHA/CUR-DAPMA (G), SAHA/CUR-SPD (H), and SAHA/CUR-SPM (I) administrations. NT = non-treated cells (green bars). Data represent the average of three independent experiments ± the standard deviation. Western blots for HDAC2 and MMP2 expression following treatments with SAHA alone and in combination with CUR-DAPMA (J), CUR-SPD (K), and CUR-SPM (L). Actin is used as control..

Photodynamic therapy (PDT) treatments

To evaluate the phototoxic potential of combined CUR or CUR-loaded NMs and blue laser treatments, the generation of ROS was also investigated. At T0, no significant induction of ROS was detected after treatment with different CUR concentrations; concomitantly, a moderate increase in ROS production was assessed by administering CUR in association with laser irradiation, particularly at high CUR concentrations (Figure 7A). This had an impact on cell viability, which reduced on combined CUR/laser treatment (Figure 7B). High ROS levels were detected in the same experiments performed at T0 with the CUR-loaded NMs. Indeed, CUR-DAPMA administration (with/without laser) resulted in significant ROS generation (Figure 7C) which, in turn, decreased cell viability (Figure 7F). The combined C_{16}-SPD or C_{16}-SPM NMs and laser irradiation treatments also resulted in a modest increase in ROS generation compared to the corresponding no-laser experiments (Figure 7D-E). Notably, C_{16}-SPD and C_{16}-SPM 1μM treatments decreased cell viability with/without laser, while treatments with these two NMs loaded with 500 nM CUR showed an increase in cell viability compared to untreated samples (Figure 7G-H).

Cell viability assays carried out after 24 h (T24) revealed that a single exposure to blue laser led to a considerably cell viability reduction *per se* (Figs. 7I-L). After CUR treatment with laser irradiation, this cell viability decline was further induced (Figure 7I) to levels comparable to those achieved upon NMs treatment without laser exposure. Low doses of CUR-loaded NM treatments combined with laser blue light dramatically reduced cell viability (Figure 7J-L). For comparison, such low cellular vitality values could be achieved only by administering high doses of free CUR (Figure 7I).

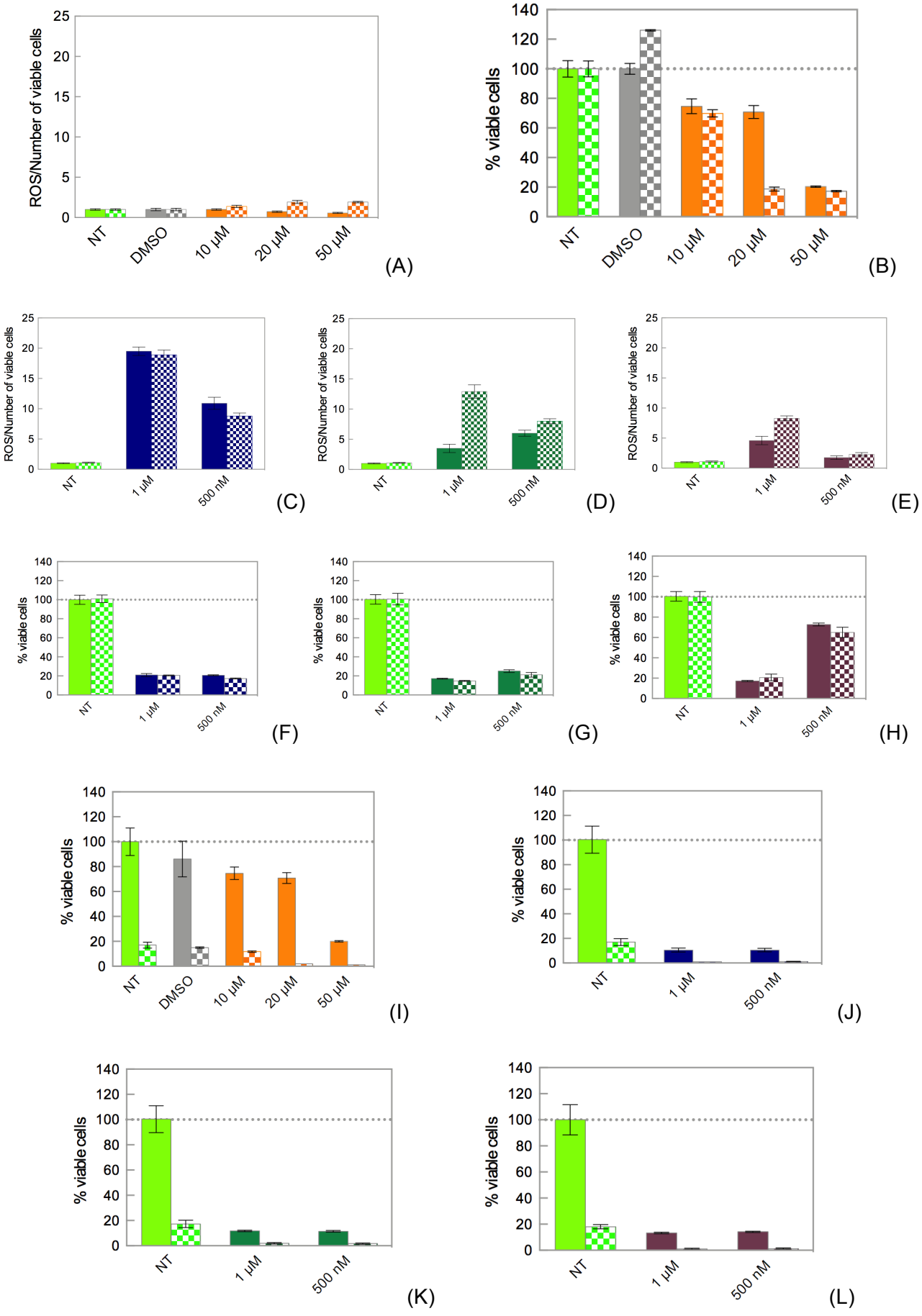

Figure 7. SFT cells treated with CUR or CUR-loaded NMs combined with PDT. Quantification of ROS generation immediately after treatment (T0) (A), and cell viability (B) after CUR alone (orange bars) and CUR/PDT combined

treatments (orange/white checked bars). T0 quantification of ROS generation (C,D,E) and cell viability (F,G,H) after CUR-DAPMA alone (dark blue bars) and CUR-DAPMA/PDT combined treatments (dark blue/white checked bars), CUR-SPD alone (dark green bars) and CUR-SPD/PDT combined treatments (dark green/white checked bars), and CUR-SPM alone (dark plum bars) and CUR-SPM/PDT combined treatments (dark plum/white checked bars). Cell viability at 24 h (T24) after CUR alone (orange bars) and CUR/PDT combined treatments (orange/white checked bars) (I), CUR-DAPMA alone (dark blue bars) and CUR-DAPMA/PDT combined treatments (dark blue/white checked bars) (J), CUR-SPD alone (dark green bars) and CUR-SPD/PDT combined treatments (dark green/white checked bars) (K), and CUR-SPM alone (dark plum bars) and CUR-SPM/PDT combined treatments (dark plum/white checked bars) (L). NT = non-treated cells. Data represent the average of three independent experiments ± the standard deviation.

Discussion

Conventional chemotherapy is effective in controlling/stabilizing locally advanced/metastatic SFTs,[6] but suffers from numerous side effects, resistance, and has not significantly improved patient survival thus far. Thus, non-toxic, more selective agents are urgently needed to treat SFTs. CUR is known to exert anti-cancer activity via its effect on several biological pathways involved in mutagenesis, oncogene expression, cell cycle regulation, apoptosis, tumorigenesis, tumor growth, angiogenesis, and metastasis.[31] Here, we explored the activity of CUR (both in its free and nanovector-encapsulated form) on a stable SFT cell line. Initially, the sensitivity of SFT cells to free CUR was evaluated *in vitro*. The results obtained show a dose-dependent reduction in cell viability upon increasing CUR concentration (Figure 2A-C); yet, a significant reduction in the expression of key EMT markers could only be achieved at high CUR doses (50 μM, Figure 2D). Unfortunately, such CUR concentrations can induce heavy side effects *in vivo*. The application of CUR-loaded NMs resulted in a drastic decrease in cell viability and expression of the EMT markers[32] at substantially lower doses of active principle with respect to free CUR administration (Figures 3 and 4). Once inside SFT cells, the three CUR-loaded NMs interact with the pathways involved in EMT in different ways. CUR-DAPMA and CUR-SPD were again the most effective NMs in reducing the expression of all EMT markers except for integrin β3 which, in the case of CUR-DAPMA, exhibited expression levels comparable to those observed in untreated samples. CUR-SPD treatments induced inhibition of all EMT protein expression at 24 h, while CUR-DAPMA treatment required at least 48 h to obtain a reduction of YY1 and c-Myc expression. Conversely, CUR-SPM treatment resulted in a decrease of YY1, c-Myc and SLUG proteins but did not affect EZH2 and

integrinβ3 expression even after 48 h (Figure 4). Notwithstanding similar CUR release profiles for the three NMs were obtained *in vitro* (Figure 2S), their distinctive chemico-physical features might induce different drug release once inside the cells, ultimately leading to distinct interactions between target proteins and CUR. It is, nonetheless, clear that molecular-scale programming of the SAMul NM delivery vehicle plays a direct role in tuning its biological performance within the cell, which suggests such systems can undergo significant structure-activity effect optimization to open up a range of potential applications against different therapeutic targets. In this case, CUR-SPD appeared to be the optimal system in terms of its activity. The observations that CUR-loaded NMs dramatically decreased the levels of EMT marker expression is encouraging, and represents an area of investigation currently in progress in our laboratories.

Results from invasion assays demonstrate that all CUR-loaded NMs were significantly more effective in inhibiting SFT cell invasion (Figure 3D-F) than CUR alone (Figure 2C). One of the key factors associated with cancer cells invasion and metastasis is the overexpression of matrix metalloproteinase2 (MMP2), an endopeptidase capable of digesting the extracellular matrix. HDAC inhibitors such as SAHA, which targets HDAC2 and MMP2, are promising therapeutic agents currently in cancer clinical trials.[33] Since the NAB2/STAT6 fusion protein interacts with HDAC2 activity in SFTs,[3,34] CUR/SAHA and CUR-loaded NMs/SAHA combined treatments of SFT cells were performed. SAHA alone or in combination with CUR did not significantly affect SFT cell viability (Figure 5A); on the other hand, SAHA induced down-regulation of MMP2 expression compared with the combined CUR treatment (Figure 5D). Similarly to EMT marker expression, the use of NMs led to a significantly stronger reduction of MMP2 expression (Figure 6J-L). In particular, CUR-SPD and CUR-SPM NMs were able to reduce the expression of MMP2 within 24h, thereby abrogating the invasion rate of SFT cells (Figure 3D-F). Low expression of MMP2 correlates with fewer tumor cells showing invasive behavior; thus, it is tempting to speculate that, should CUR-SPD and CUR-SPM NMs be able to suppress MMP2 expression *in vivo*, this might translate into inhibited SFT cell invasive behavior and reduced potential for metastasis. According

to the results in Figure 5L, CUR-DAPMA seemed to have a greater impact on HDAC2 expression (24 h) than on MMP2 expression (48 h). Therefore, we suggest that CUR-DAPMA NMs and SAHA might be likely involved in a synergistic inhibition of HDAC2.

The most interesting and unexpected effect of SAHA treatment was the morphological change of the tumor cells. After treatment with SAHA alone or in combination treatments, SFT cells exhibited a more epithelial-like shape (Figure 5B). Previous studies demonstrated that SAHA treatment can induce morphological changes in an osteosarcoma cell line and reduce invasiveness.[35] Here, the cytotoxic activity of CUR-loaded NMs (Figure 6D-F) prevented the detection of cytoskeleton variations as observed in the previous experiments with free SAHA and CUR. SAHA trials in patients with solid tumors have produced conflicting results,[36] in which this compound exerts both pro- and anti-apoptotic pathways. However, based on the evidence that SAHA stabilizes disease and elicits partial responses in patients, SAHA remains in clinical trials as a component of multi-drug therapies.[37] Our data unambiguously show that SAHA could inhibit markers of metastasis (MMP2) and SFT cell invasiveness in CUR-SPD and CUR-SPM NMs combined treatments, while the SAHA/CUR-DAPMA combination tended to increase the aggressive behavior of cancer cells. Once again, CUR-SPD emerges as a promising delivery system, this time in combination with SAHA. These results undoubtedly deserve further studies aimed at defining the specific pathways activated by each MN type. In addition, the effect of SAHA should be tested on other sarcoma cell lines to determine an eventual rationale, still unknown, able to explain how SAHA can induce both pro- and anti-apoptotic pathways.

The use of photodynamic therapy (PDT) is steadily growing as an innovative/promising approach in cancer therapeutics. Generally, the systemic toxicity of chemotherapeutic drugs can be reduced using PDT[38] which is employed in order to activate the cytotoxic effect at the desired site of action. Specifically, Koon and colleagues reported that CUR cytotoxicity is enhanced by blue light laser application in nasopharyngeal cancer cell lines[39] by virtue of the drug's potential to generate reactive oxygen species (ROS) on irradiation[40] which, in turn, plays an important role in controlling

proliferation and apoptosis.[41] In the last part of this study we investigated the combined effect of PDT and CUR administrations on cell viability using both free and NM-encapsulated drug. SFT cells were found to be more sensitive to the combined CUR/PDT treatments, which exerted a specific reduction of proliferative potential. Treating SFT cells using CUR doses of up to 50 μM in combination with laser revealed a concentration-dependent viability reduction immediately after irradiation (Figure 7A-B). Experiments carried out using PDT and CUR-loaded NMs combination treatment resulted in almost complete cell viability abrogation 24 h after laser irradiation (Figure 7J-L) at much lower CUR concentrations, demonstrating the potential of these NM delivery vehicles to be effectively combined with PDT.

In summary, the present study establishes the importance of adopting effective nanocarrier systems to efficiently deliver CUR to SFT cells, achieve substantial cytotoxic activity, affect EMT markers expression and decrease cancer cell invasiveness. Intriguingly, the molecular-scale programming of the surface ligands on the NM delivery vehicle, changes which are relatively subtle in nature, significantly modified the biological activity, with CUR-SPD generally being the most effective system. In combination with SAHA, CUR-SPD suppressed MMP2 expression, lowering the aggressive nature of the tumor, and hence its metastatic potential. Moreover, an approach based on combining CUR-loaded NMs and blue laser PDT treatment led to very promising results, with laser light addition resulting in almost complete loss of cell viability when using CUR-NM delivery systems. Since the proposed NM formulations showed great potential *in vitro*, further studies focusing on determining the mechanisms underlying the different pharmacological response and EMT marker expression inhibition elicited by our CUR-loaded NMs are currently ongoing in our laboratories and will be reported soon. If successful, these studies will warrant future investigations establishing pharmacokinetic profile and cytotoxic effects of these systems *in vivo* (i.e., animal models). Finally, it is also worth noting that in addition to binding a drug such as CUR in the hydrophobic interior, the surface ligands of these NMs can be used to bind biomolecular drug cargoes (e.g. nucleic acids). This opens the potential of dual therapies in which such carriers are

used to deliver two different active agents into tumor cells. Work towards such multidrug therapies is currently underway.

Supporting information

Size distribution (DLS) of CUR-DAPMA, CUR-SPD, and CUR-SPM nanomicelles (Figure S1); Average nanomicelles diameters, zeta potential, drug encapsulation efficiency and drug loading CUR-DAPMA, CUR-SPD, and CUR-SPM nanomicelles (Table S1); *in vitro* release behavior from free CUR, CUR-DPMA, CUR-SPD, and CUR-SPM nanomicelles (Figure S2); Western blots for HDAC2 and MMP2 expression following CUR-DAPMA, CUR-SPD, and CUR-SPM treatments.

Acknowledgements

This work was supported by a PROMOS scholarship from Freie Universität Berlin to LEF. The generous research financial support from the Italian Association for Cancer Research (AIRC, Grant IG 17413 to SP) is gratefully acknowledged.

References

1. Travis, W.D.; Churg, A.; Aubry, M.C.; Ordonez, N.G.; Tazelaar, H.; Pugatch, R.; *et al*. Mesanchymal tumors. In: *Tumors of the lung, pleura, thymus and heart*; Travis, W.D., Brambilla, E., Müller-Hermelink, H.K., Harris, C.C., Eds.; IARC Press: Lyon, 2004, pp 142-143.

2. Vilanova, J.C. WHO classification of soft tissue tumors. In: *Imaging of soft tissue tumors*; de Schepper, A.M., Vanhoenacker, F.M., Parizel, P.M., Gielen, J.L., Eds.; Springer-Verlag: Berlin, 2017, pp 187-196.

3. Chmielecki, J.; Crago, A.M.; Rosenberg, M.; O'Connor, R.; Walker, S.R.; Ambrogio, L.; *et al.* Whole-exome sequencing identifies a recurrent NAB2-STAT6 fusion in solitary fibrous tumors. *Nat. Genet*. **2013**, *45*, 131-132.

4. Gold, J.S.; Antonescu, C.R.; Hajdu, C.; Ferrone, C.R.; Hussain, M.; Lewis, J.J.; *et al.* Clinicopathologic correlates of solitary fibrous tumors. *Cancer* **2002**, *94*, 1057-1068.

5. Stacchiotti. S.; Marrari, A.; Dei Tos, A.P.; Casali, P.G. Targeted therapies in rare sarcomas: IMT, ASPS, SFT, PEComa, and CCS. *Hematol. Oncol. Clin. North. Am*. **2013**, *27*, 1049-1061.

6. Stacchiotti, S.; Libertini, M.; Negri, T.; Palassini, E.; Gronchi, A.; Fatigoni, S.; *et al*. Response to chemotherapy of solitary fibrous tumor: a retrospective study. *Eur. J. Cancer* **2013**, *49*, 2376-2383.

7. Stacchiotti, S.; Negri, T.; Libertini, M.; Palassini, E.; Marrari, A.; De Troia, B.; *et al*. Sunitinib malate in solitary fibrous tumor (SFT). *Ann. Oncol*. **2012**, *23*, 3171-3179.

8. Valentin, T.; Fournier, C.; Penel, N.; Bompas, E.; Chaigneau, L.; Isambert, N.; *et a*l. Sorafenib in patients with progressive malignant solitary fibrous tumors: a subgroup analysis from a phase II study of the French Sarcoma Group (GSF/GETO). *Invest. New Drugs* **2013**, *31*, 1626-1627.

9. Stacchiotti, S.; Tortoreto, M.; Baldi, G.G.; Grignani, G.; Dei Toss, A.P.; Badalamenti, G.; *et al*. Preclinical and clinical evidence of activity of pazopanib in solitary fibrous tumor. *Eur. J. Cancer* **2014**, *50*, 3021-3028.

10. Park, M.S.; Patel, S.R.; Ludwig, J.A.; Trent, J.C.; Conrad, C.A.; Lazar, A.J.; *et al*. Activity of temozolomide and bevacizumab in the treatment of locally advanced, recurrent, and metastatic hemangiopericytoma and malignant solitary fibrous tumor. *Cancer* **2011**, *117*, 4939-47.

11. Spagnuolo, R.D.; Brich, S.; Bozzi, F.; Conca, E.; Castelli, C.; Tazzari, M.; *et al*. Sunitinib-induced morpho-functional changes and drug effectiveness in malignant solitary fibrous tumors. *Oncotarget* **2016**, *7*, 45015-45026.

12. Phi, L.T.H.; Sari, I.N.; Yang, Y.G.; Lee, S.H.; Jun, N.; Kim, K.S.; *et al*. Cancer stem cells (CSCs) in drug resistance and their therapeutic implications in cancer treatment. *Stem Cells Int*. **2018**, 5416923.

13. Zhihong. C.; Yijing, C.; Yichen, L.; Haobin, H.; Hui, L. Signaling mechanism(s) of epithelial-mesenchymal transition and cancer stem cells in tumor therapeutic resistance. *Clin. Chim. Acta* **2018**, *483*, 156-163.

14. Panda, A.K.; Chakraborty, D.; Sarkar, I.; Khan, T.; Sa, G. New insights into therapeutic activity and anticancer properties of curcumin. *Exp. Pharmacol*. **2017**, *9*, 31-45.

15. Feitelson, M.A.; Arzumanyan, A.; Kulathinal, R.J.; Blain, S.W.; Holcombe, R.F.; Mahajna, J.; *et al*. Sustained proliferation in cancer: mechanisms and novel therapeutic targets. *Semin. Cancer Biol*. **2015**, *35*, S25-S54.

16. Anand, P.; Kunnumakkara, A.B.; Newman, R.A.; Aggarwal, B.B. Bioavailability of curcumin: problems and promises. *Mol. Pharm*. **2007**, *4*, 807-818.

17. Naksuriya, O.; Okonogi, S.; Schiffelers, R.M.; Hennink, W.E. Curcumin nanoformulations: a review of pharmaceutical properties and preclinical studies and clinical data related to cancer treatment. *Biomaterials* **2014**, *35*, 3365-3383.

18. Gera, M.; Sharma, N.; Ghosh, M.; Huynh, D.L.; Lee, S.J.; Min, T.; *et al*. Nanoformulations of curcumin: an emerging paradigm for improved remedial application. *Oncotarget* **2017**, *8*, 66680-66698.

19. Wei, T.; Chen, C.; Liu, J.; Liu, C.; Posocco, P.; Liu, X.; *et al*. Anticancer drug nanomicelles formed by self-assembling amphiphilic dendrimer to combat cancer drug resistance. *Proc. Natl.*

Acad. Sci. USA **2015**, *112*, 2978-2983.

20. Barnard, A.; Posocco, P.; Pricl, S.; Calderon, M.; Haag, R.; Hwang, M.E.; *et al*. Degradable self-assembling dendrons for gene delivery: Experimental and theoretical insights into the barriers to cellular uptake. *J. Am. Chem. Soc*. **2011**, *133*, 20288-20300.

21. Barnard. A.; Posocco, P.; Fermeglia, M.; Tschiche, A.; Calderon, M.; Pricl, S.; *et al*. Double-degradable responsive self-assembled multivalent arrays-temporary nanoscale recognition between dendrons and DNA. *Org. Biomol Chem*. **2014**, *12*, 446-455.

22. Bromfield, S.M.; Posocco, P.; Chan, C.W.; Calderon, M.; Guimond, S.E.; Turnbull, J.E.; *et al*. Nanoscale self-assembled multivalent (SAMul) heparin binders in highly competitive, biologically relevant, aqueous media. *Chem. Sci*. **2014**, *5*, 1484-1492.

23. Fechner, L.E.; Albanyan, B.; Vieira, V.M.P.; Laurini, E.; Posocco, P.; Pricl, S.; *et al*. Electrostatic binding of polyanions using self-assembled multivalent (SAMul) ligand displays-structure-activity effects on DNA/heparin binding. *Chem. Sci*. **2016**, *7*, 4653-4659.

24. Chan, C.W.; Laurini, E.; Posocco, P.; Pricl, S.; Smith, D.K. Chiral recognition at self-assembled multivalent (SAMul) nanoscale interfaces-enantioselectivity in polyanion binding. *Chem. Commun*. **2016**, *52*, 10540-10543.

25. Albanyan, B.; Laurini, E.; Posocco, P.; Pricl, S.; Smith, D.K. Self-assembled multivalent (SAMul) polyanion binding - impact of hydrophobic modifications in the micellar core on DNA and heparin binding at the peripheral cationic ligands. *Chem. Eur. J*. **2017**, *23*, 6391-6397.

26. Rodrigo, A.C.; Bromfield, S.M.; Laurini, E.; Posocco, P.; Pricl, S.; Smith, D.K. Morphological control of self-assembled multivalent (SAMul) heparin binding in highly competitive media. *Chem. Commun*. **2017**, *53*, 6335-6338.

27. Eckschlager, T.; Plch, J.; Stiborova, M.; Hrabeta, J. Histone deacetylase inhibitors as anticancer drugs. *Int. J. Mol. Sci*. **2017**, *18*, 1414.

28. Chilakamarthi, U.; Giribabu, L. Photodynamic therapy: past, present and future. *Chem. Rec*. **2017**, *17*, 775-802.

29. Hall, D.M.; Brooks, S.A. In vitro invasion assay using matrigel™: a reconstituted basement membrane preparation. *Methods Mol. Biol*. **2014**, *1070*, 1-11.

30. Miselli, F.; Negri, T.; Gronchi, A.; Losa, M.; Conca, E.; Brich, S.; *et al*. Is autophagy rather than apoptosis the regression driver in imatinib-treated gastrointestinal stromal tumors? *Transl. Oncol*. **2008**, *1*, 177-186.

31. Wilken, R.; Veena, M.S.; Wang, M.B.; Srivatsan, E.S. Curcumin: a review of anti cancer properties and therapeutic activity in head and neck squamous cell carcinoma. *Mol. Cancer* **2011**, *10*, 12.

32. Lamouille, S.; Xu, J.; Derynck, R. Molecular mechanisms of epithelial–mesenchymal transition.

Nat. Rev. Mol. Cell. Biol. **2014**, *15*, 178-196.

33. Shankar, S.; Davis, R.; Singh, K.P.; Kurzrock, R.; Ross, D.D.; Srivastava, R.K. Suberoylanilide hydroxamic acid (Zolinza/vorinostat) sensitizes TRAIL-resistant breast cancer cells orthotopically implanted in BALB/c nude mice. *Mol. Cancer. Ther*. **2009**, *8*, 1596-1605.

34. Robinson, D.R.; Wu, Y.M.; Kalyana-Sundaram, S.; Cao, X.; Lonigro, R.J.; Sung, Y.S.; *et al*. Identification of recurrent NAB2-STAT6 gene fusions in solitary fibrous tumor by integrative sequencing. *Nat. Genet*. **2013**, *45*, 180-185.

35. Mu, X.; Brynien, D.; Weiss, K.R. The HDAC inhibitor Vorinostat diminishes the in vitro metastatic behavior of osteosarcoma cells. *Biomed. Res. Int*. **2015**, *2015*, 290368.

36. Luu, T.H.; Morgan, R.J.; Leong, L.; Lim, D.; McNamara, M.; Portnow, J.; *et al.* A phase II trial of vorinostat (suberoylanilide hydroxamic acid - SAHA) in metastatic breast cancer: a california cancer consortium study. *Clin. Cancer Res*. **2008**, *14*, 7138-7142.

37. Marks, P.A.; Breslow, R. Dimethyl sulfoxide to vorinostat: development of this histone deacetylase inhibitor as an anticancer drug. *Nat. Biotechnol*. **2007**, *25*, 84-90.

38. Sarkar, F.H.; Li, Y.W. Targeting multiple signal pathways by chemopreventive agents for cancer prevention and therapy. *Acta Pharmacol. Sin.* **2007**, *28*, 1305-1315.

39. Koon, H.; Leung, A.W.; Yue, K.K.; Mak, N.K. Photodynamic effect of curcumin on NPC/CNE2 cells. *J. Environ. Pathol. Toxicol. Oncol*. **2006**, *25*, 205-216.

40. Bruzell, E.M.; Morisbak, E.; Tonnesen, H.H. Studies on curcumin and curcuminoids. XXIX. Photoinduced cytotoxicity of curcumin in selected aqueous preparations. *Photochem. Photobiol. Sci*. **2005**, *4*, 523-530.

41. Thannickal, V.J.; Fanburg, B.L. Reactive oxygen species in cell signaling. *Am. J. Physiol. Lung Cell. Mol. Physiol*. **2000**, *279*, L1005-L1028.

For Table of Content Use Only